ChemPubSoc Europe

DOI: 10.1002/cphc.201300856

VIP

On the Electrochemical Deposition and Dissolution of Divalent Metal Ions

Leandro M. C. Pinto,[a, b] Paola Quaino,[c] Elizabeth Santos,[a, d] and Wolfgang Schmickler*[a]

The deposition of Cu^{2+} and Zn^{2+} from aqueous solution has been investigated by a combination of classical molecular dynamics, density functional theory, and a theory developed by the authors. For both cases, the reaction proceeds through two one-electron steps. The monovalent ions can get close to the electrode surface without losing hydration energy, while the divalent ions, which have a stronger solvation sheath, cannot. The 4s orbital of Cu interacts strongly with the sp band and more weakly with the d band of the copper surface, while the Zn 4s orbital couples only to the sp band of Zn. At the equilibrium potential for the overall reaction, the energy of the intermediate Cu^{+} ion is only a little higher than that of the divalent ion, so that the first electron transfer can occur in an outer-sphere mode. In contrast, the energy of the Zn^{+} ion lies too high for a simple outer-sphere reaction to be favorable; in accord with experimental data this suggests that this step is affected by anions.

1. Introduction

During the last decade, there has been a significant rise in development of theoretical electrochemistry. Because of the urgent energy problems of our age, the vast majority of these works are devoted to electrocatalysis and fuel-cell reactions. In contrast, the field of metal deposition and dissolution has been almost neglected by theoreticians, even though it is also of huge economic importance: It forms the basis of electrowinning and plating, and of corrosion, which every year costs thousands of billions of dollars. In addition, the deposition/dissolution of a metal ion is one of the few fundamental processes of electrochemistry, and it is a challenge to understand it from an atomistic point of view.

Already in the 1990s one of us developed a general framework for a quantum theory of electrodeposition.[1,2] However, at that time density function theory (DFT) and similar quantum-chemical methods were computationally too costly to be applied to metal surfaces. Therefore, subsequent applications and extensions of this work[3–5] suffered from a lack of knowledge of the electronic interactions between the metal ions and the electrode. Recently, we have taken up this line of research again and shown how it can be combined with DFT and with classical molecular dynamics simulations to form a complete model for metal deposition. Our first application was to the deposition of silver, which is one of the fastest electrochemical reactions.[6] From our theory we calculated the free-energy surface for silver deposition on a terrace and showed that, at zero overpotential, the energy of activation is lower than that for the subsequent incorporation of silver into a kink site, which is in accord with experimental data.[7] The high rate of the deposition was traced to two effects: 1) In aqueous solutions, small metal ions such as Ag^{+} can get very close to the electrode surface without losing hydration energy; 2) the Ag 5s orbital interacts strongly with the silver sp band.

We surmise that the first effect generally holds for small metal ions; however, the situation is quite different for multivalent ions. Pecina and Schmickler[8] showed that the energy of the Zn^{2+} ion rises rapidly when it loses its secondary solvation shell, which happens a few Ångstroms from the electrode surface. In addition, Marcus theory[9] suggests that the simultaneous transfer of two electrons is unlikely, so that the deposition of multivalent ions should happen in a series of one-electron steps. There are thus good reasons to investigate the deposition of multivalent ions.

In this work, we have chosen two model systems: the depositions of Cu^{2+} and Zn^{2+}. We show that the ions exhibit both similarities and important differences.

The paper is organized as follows: First, we investigate the approach of the ions to the surface by classical molecular dynamics, and then their electronic interactions with the electrode. We then use this information to calculate the kinetics of deposition, by treating each ion in turn. All technical details can be found in the Technical Section.

[a] Dr. L. M. C. Pinto, Dr. E. Santos, Prof. Dr. W. Schmickler
Institute of Theoretical Chemistry
Ulm University
Helmholtzstrasse, 89069 Ulm (Germany)
E-mail: wolfgang.schmickler@uni-ulm.de

[b] Dr. L. M. C. Pinto
Faculdade de Ciências
Universidad Estadual Paulista, UNESP
17.033-360 Bauru-SP (Brazil)

[c] Dr. P. Quaino
Programa de Electroquímica Aplicada e
Ingeniería Electroquímica (PRELINE)
Universidad Nacional del Litoral
Santa Fe (Argentina)

[d] Dr. E. Santos
Faculdad de Matemática, Astronomía y Física
IFEG-CONICET, Universidad Nacional de Córdoba
Córdoba (Argentina)

2. Approach to the Electrode Surfaces

Like all divalent ions, Cu^{2+} and Zn^{2+} have high energies of hydration; $\Delta G_{sol}(Cu^{2+}) = -21.77$ eV and $\Delta G_{sol}(Zn^{2+}) = -21.28$ eV.[10] For copper a value for the monovalent ion is also available from the literature; $\Delta G_{sol}(Cu^{+}) = -6.33$ eV[10]; we calculated the corresponding value for zinc by using molecular dynamics simulations (see the Experimental Section), and obtained a value of $\Delta G_{sol}(Zn^{+}) = -5.69$ eV.

If an ion moves from the bulk of the solution towards the electrode surface, the number of water molecules in its immediate surroundings decreases and the hydration energy of the ion changes. The corresponding change, as a function of the distance from the electrode, is called the potential of mean force (pmf), and can be calculated by using molecular dynamics within a given model. Pecina and Schmickler[4] have performed such calculations for the two zinc ions, whereas we now also treated the copper ions. The results for all four ions are shown in Figure 1. Just like Ag^{+}, the monovalent ions Zn^{+} and Cu^{+} can get very close to the electrode surface without losing solvation energy. There is even a slight energy minimum next to the surface. As we have discussed before,[6] at these minima water forms a very effective solvation cage for such small metal ions. As water at the surface has fewer hydrogen bonds than in the bulk, it is free to orient its dipole moment in accord with the Coulomb force of the ions. The electrode surface also helps to align the water molecules in a favorable orientation. A picture of a metal ion in its solvation cage at the surface is shown in ref. [6]. We note that these metal ions behave quite differently from a halide ion, which loses a large part of its solvation energy as it approaches an electrode surface.[11,12]

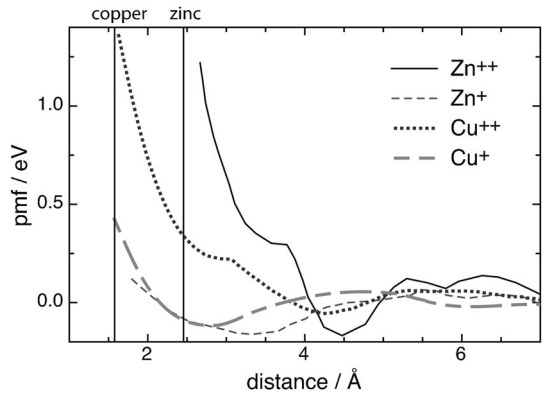

Figure 1. Potentials of mean force (pmf) for the approach of ions from the bulk of an aqueous solution towards an electrode surface: Zn^{+} and Zn^{2+} towards Zn(0001), Cu^{+} and Cu^{2+} to Cu(100). The potentials refer only to the interaction of the ions with the solvent. The data for Zn deposition are taken from ref. [8]. The vertical lines indicate the position of the deposited copper and zinc atoms. The distances are given with respect to the top layer of metal atoms.

For the divalent ions the situation is quite different. Their pmfs also exhibit a minimum, but at a larger distance from the surface. When the ions approach further, they start to shed their secondary solvation shells, and their free energy rises. Therefore, a close approach of the divalent ions to the surface is energetically very unfavorable.

3. Electronic Interaction between Reactant and Electrode

In order to investigate the electronic interactions we performed DFT calculations for various distances of the Cu and Zn atoms from their respective surfaces. Figure 2 shows some of the electronic densities of states (DOS) obtained, which help to understand these interactions. If the copper atom is a few Ångstroms from the surface (Figure 3), its DOS is centered at the Fermi level and contains one 4s electron. If it has been deposited, its DOS is very broad and overlaps with those of the sp and the d band. Note that the d band lies only a little below the Fermi level, and therefore participates in the bonding. The strengths of these interactions are detailed below.

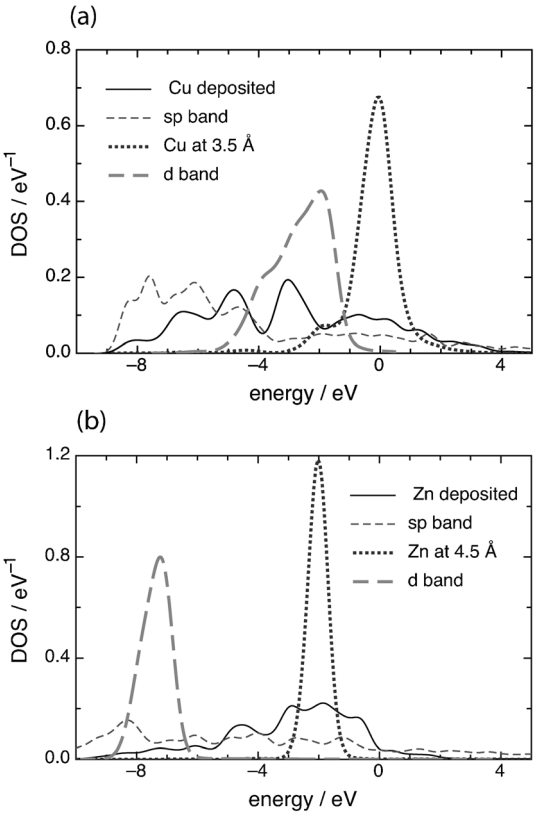

Figure 2. Electronic density of states of the valence orbitals of a) a copper atom and b) a zinc atom in the deposited state and at some distance from the surface. The d and sp bands of the metal surfaces are also shown.

The valence-electron configuration of the Zn atom is $4s^2$; therefore, its DOS is centered well below the Fermi level when it is a few Ångstroms from the surface. In the deposited state, the DOS of the Zn atom is also broadened and overlaps with the sp band, as is the case for copper. The zinc d band lies too low to play any role.

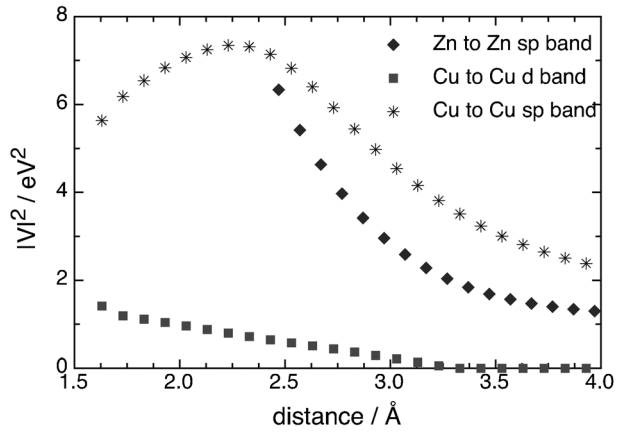

Figure 3. Coupling constant of the 4s orbital of Cu and Zn to their respective surfaces.

By using the fitting procedure described in ref. [13], we obtained the coupling constants between the 4s orbitals of Cu and Zn and their respective surfaces. The copper atom interacts both with the copper sp and d band, but the coupling with the former is stronger. At short distances, the interaction with the sp band becomes somewhat weaker, and that with the d band stronger, so that the total interaction is roughly constant. The Zn 4s orbital does not interact with the d band, but the coupling with the sp band is strong and rises as the atom approaches the electrode surface. For both metals, the interaction with the electrode is about as strong as in the case of silver, and is dominated by the sp band.

4. Kinetics of Metal Deposition

By combining the results of DFT and the molecular dynamics simulations, we can calculate the free-energy surfaces for the reactions by using our theory. The calculations follow the method that we developed for hydrogen evolution,[13] which we improved in two points: 1) We calculated the interaction with the sp band by using DFT and 2) from the simulations, we directly obtain the interaction of the ion with the solvent. The total interaction, as a function of the distance, is given by the sum of the free energy of hydration of the ion in the bulk and the pmf, as shown in Figure 1. This energy is then split into the slow part, which gives the energy of reorganization as a function of the distant, and a fast, electronic part. Further details are given in the Technical Section. We treat both reactions in turn.

4.1. Copper Deposition

The Cu^+ ion is not stable in aqueous solutions, but the redox potentials for both ions are available [Eqs. (1)–(3)]:[10]

$$Cu^{2+} + 2e^- \rightleftharpoons Cu \quad 0.340\ V \qquad (1)$$

$$Cu^{+} + e^- \rightleftharpoons Cu \quad 0.520\ V \qquad (2)$$

$$Cu^{2+} + e^- \rightleftharpoons Cu^{+} \quad 0.159\ V \qquad (3)$$

From the pmfs shown in Figure 1 it is evident that the Cu^{2+} ion cannot approach the surface. Therefore the first electron-transfer step takes place in an outer-sphere mode. At the equilibrium potential for the overall reaction [Eq. (1)], this step is endergonic by $\Delta G = 0.18$ eV. The energy of reorganization λ for this step can be estimated from the energy of solvation. In aqueous solution the Pekar[14] factor is $(1/\varepsilon_s - 1/\varepsilon_\infty) \approx 1/2$, where ε_s is the static and ε_∞ the optical dielectric constant. By assuming that the solvation energy scales with the square of the charge number z, we estimate [Eq. (4)]:

$$\Delta G_{sol} \approx -2\lambda z^2 = -21.77\ \text{eV}$$
$$\text{hence } \lambda \approx 2.72\ \text{eV} \qquad (4)$$

From Marcus theory, we then obtain for the energy of activation for the first electron-transfer step Equation (3) at the equilibrium potential of the overall reaction [Eq. (1)], as shown in Equation (5):

$$\Delta G_{act} = \frac{(\lambda + \Delta G)^2}{4\lambda} \approx 0.77\ \text{eV} \qquad (5)$$

Of course, this estimate is somewhat rough: Energies of solvation do not quite scale with z^2, and the Marcus free-energy curves are really not quite parabolic.[15] However, it is good enough to show that the first step occurs with a decent velocity in an outer-sphere mode.

In the second step, the Cu^+ ion is discharged and deposited onto the terrace. We have calculated the free-energy surface for this step as a function of the distance of the reactant from the electrode and the solvent coordinate q. The latter concept, originally introduced by Marcus and Hush,[9,16] characterizes the state of the solvent. In our normalization[17] the solvent is in a state characterized by q if it is in equilibrium, with a reactant of charge $-q$. Figure 4 shows the surface for the case in which the Cu^{2+} ion in solution is in equilibrium with the kink

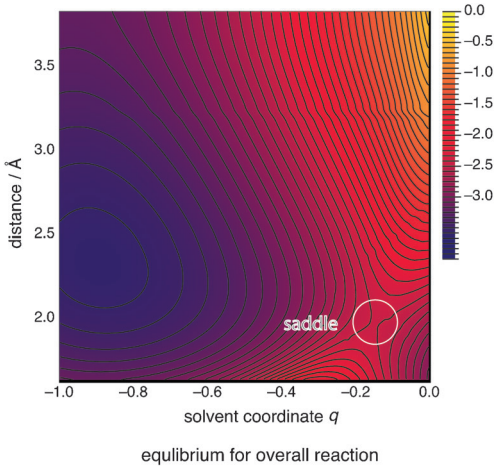

Figure 4. Free-energy surface for the reaction: $Cu^{2+} + e^- \rightarrow Cu$, where the final state is an atom deposited on the terrace. The calculations were performed for the case in which the overall reaction [Eq. (1)] is in equilibrium, that is, the Cu^{2+} is in equilibrium with the kink site. Note that the energy of the terrace site is about 0.45 eV higher than that of the kink site.

site, which is the overall equilibrium for the total reaction shown in Equation (1). As the energy of the terrace site is about 0.45 eV higher than at the kink site, the deposition onto the terrace is endergonic. The surface shows a minimum at $q=-1$ and a distance of about 2.5 Å, which corresponds to the copper ion that is situated at the minimum in the pmf depicted in Figure 1. A second minimum at $q=0$ and right on the surface belongs to the metal atom deposited on the terrace. The minima are separated by a saddle point and the corresponding energy of activation, with respect to the Cu^{2+} ion in solution, is about 0.68 eV. Finally, we also calculated the energy of activation to go from the terrace to the kink site; with respect to the terrace, this has a value of 0.3 eV, and with respect to the initial state this would be 0.75 eV. Thus, our calculations suggest that the first electron transfer is a little slower than the second, and that the migration to the kink site may also affect the rate. The activation energies are higher than for silver deposition, for which we obtained activation energies of 0.39 eV for the charge transfer (at equilibrium) and 0.57 eV for migration to the kink.

Direct comparison of our calculations with experimental data is not straightforward, as the latter depend on the state of the surface; its roughness, number of steps and kink sites, while our calculations are for a single-crystal surface. There seem to be more studies of the deposition of copper on mercury with amalgam formation than of copper on single-crystal surfaces, as the problem of the surface structure does not arise for amalgam formation. However, studies of copper on copper do suggest that the reaction rate is much slower than for the deposition of silver on silver, and that the first electron transfer $Cu^{2+}e^{-}\rightarrow Cu^{+}$ is rate-determining.[18,19] Both findings are in line with our results. No effect of migration to the kink site was observed in the experiments. However, the rate of this step strongly depends on the state of the surface, which in all experiments is polycrystalline, whereas our value is for a single-crystal surface.

4.2. Zinc Deposition

For zinc deposition the thermodynamic data for the univalent ion are not available. However, as mentioned above, we calculated the hydration energy of this ion as $\Delta G_{sol}(Zn^{+})=-5.69$ eV. As our simulations give a good value for the divalent ion, this value should be at least a good approximation. It is reasonable that the absolute value is somewhat lower than that of Cu^{+} (−6.33 eV), since it still has one 4s electron and hence a bigger radius. By going through an appropriate Born–Haber cycle[20] we calculated the standard free energy of the intermediate Zn^{+} and obtained a value that is about 1.26 eV higher than that for the Zn^{2+} ion, with a probable error margin of ±0.2 eV. The large difference in the energies of the monovalent copper and zinc ions is easily traced to the first energy of ionization, which for copper is 7.72 eV, and for zinc is 9.39 eV.[10] Copper has one 4s electron, which is easier to detach than one of the two 4s electrons of zinc.

From the calculated values, we obtain the following reaction scheme for zinc deposition [Eqs. (6)–(8)]:

$$Zn^{2+}+2e^{-} \rightleftharpoons Zn \qquad -0.76\ \text{V (experimental)} \qquad (6)$$

$$Zn^{+}+e^{-} \rightleftharpoons Zn \qquad -0.50\ \text{V (calculated)} \qquad (7)$$

$$Zn^{2+}+e^{-} \rightleftharpoons Zn^{+} \qquad -2.05\ \text{V (calculated)} \qquad (8)$$

By using the same procedure as for copper, we estimate the energy of reorganization of the Zn^{+}/Zn^{2+} couple as 2.66 eV, which is of the same order of magnitude as that for Cu^{+}/Cu^{2+}. From the Marcus formula, we obtain an energy of activation of $E_{act}=1.44$ eV at the equilibrium potential for the overall reaction. Such a high value of E_{act} implies that zinc deposition should be extremely slow; the direct transfer of two electrons, as discussed by Gileadi,[21,22] requires an activation energy of $E_{act}=2.66$ eV, which is even worse. Nevertheless, zinc deposition does take place experimentally, and especially the deposition of zinc on mercury with subsequent amalgam formation has been well investigated.[23] We return to this point below.

From our theory we calculated the free-energy surface for the overall reaction $Zn^{2+}+2e^{-}\rightarrow Zn$ (see Figure 5a) and the corresponding occupancy of the Zn 4s orbital (Figure 5b). As both electrons belong to the same 4s orbitals, these calcula-

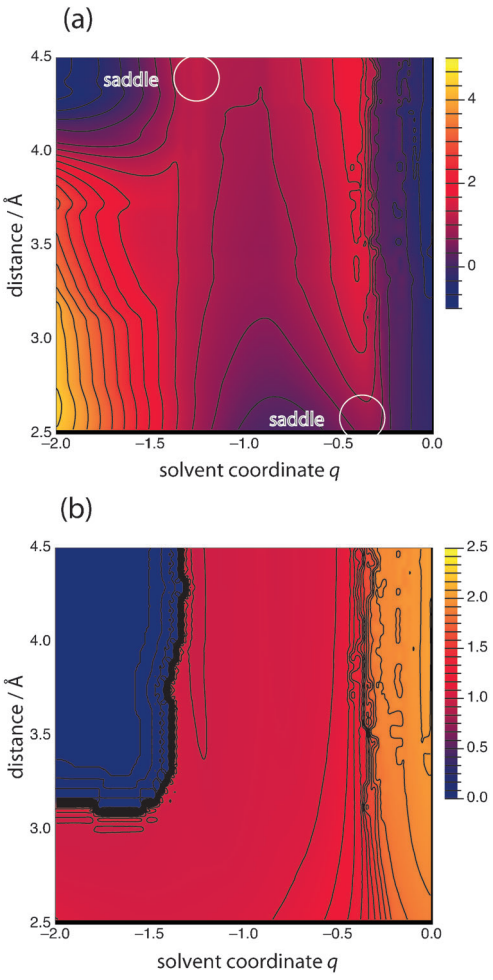

Figure 5. a) Free-energy surface for the reaction: $Zn^{2+}+2e^{-}\rightarrow Zn$, where the final state is an atom deposited on the terrace. The calculations were performed for the case in which the overall reaction is in equilibrium, that is, the Zn^{2+} is in equilibrium with the kink site. b) Occupation of the 4s orbital.

tions have been performed with spin polarization, and for the case in which the overall reaction is in equilibrium, that is, when the Zn^{2+} ion is in equilibrium with the kink site. As shown in Figure 5b, the surface shows a two-step electron transfer via Zn^{+} as an intermediate, which is in accord with our considerations above. Three main regions can be distinguished: the Zn^{2+} is stable roughly in the region $q<-1.5$ and at distances larger than about 3.2 Å; a closer approach is inhibited by the break-up of the solvation shell (see Figure 1). The uncharged atom is stable roughly in $q>-0.5$, and the univalent ion elsewhere. The energy of the univalent ion is so high that it is never absolutely stable, but only metastable near $q=-1$.

The free energy shows a saddle point at large distances and $q\approx-1.3$ corresponds to the first electron transfer. The energy of activation is the same as that calculated from Marcus theory, about 1.45 eV. The second saddle point, almost at the surface and near $q\approx-0.4$, is for the second electron transfer and has an activation energy of 1.3 eV with respect to the Zn^{2+} in solution, which is only a little higher than the energy of the Zn^{+} ion at great distances. The energy of a zinc atom deposited on the terrace is about 0.35 eV higher than at the kink site. Migration from the terrace to the kink does not require energy of activation, so overall the first electron transfer determines the rate.

Most experiments for zinc deposition have been performed on other metals such as mercury or gallium, with which amalgams or alloys are formed. In all cases, two separate electron-transfer steps were observed. Since these reactions have different equilibrium potentials, and refer to different surfaces, a detailed comparison with our calculations is not possible. However, in view of the high activation energy which we obtained for the first electron transfer, the question is why zinc deposition takes place at all. We believe that our results rule out a simple outer-sphere mechanism for the first step. Indeed, experimental results from Sluyters and co-workers[23] show that the rate constants for the formation of zinc amalgam depend strongly on the anion and vary by several orders of magnitude. These results could indicate that the rate is enhanced by anion adsorption, as the authors suggest, or by ion pairing. Obviously, more research is needed to determine the details of this mechanism.

5. Conclusions

We have investigated the deposition of two divalent ions, copper and zinc, by a combination of molecular dynamics, DFT, and our own theory. The two metals, which are neighbors in the periodic table, have a number of features in common, but differ in other aspects. The approach from the bulk of the solution to the electrode surface is the same: the monovalent ions can get very close to the surface without losing energy, while the divalent ions cannot. Also, for both reactions the discharge takes place in a series of single-electron-transfer steps. However, the different configurations of the valence electrons entail important differences. As the first ionization energy of Cu is low, the energy of the intermediate Cu^{+} is only a little higher than that of Cu^{2+}. As a consequence, Cu^{+} is a favorable intermediate state that can be accessed by an outer-sphere electron transfer. In contrast, the $4s^2$ configuration of Zn entails a higher ionization energy, and the energy of the intermediate Zn^{+} is too high to be favorable. This fact should preclude an outer-sphere mechanism for the first electron transfer, and indicates participation of anions.

A detailed comparison of our theory with experimental results would require experiments on a well-defined single-crystal surface, which are not available. However, our work does explain the differences between the deposition reactions of Ag, Cu, and Zn, and the calculated activation energies for Cu are in line with experimental data. For Zn, experiments also indicate a large effect of anions on the rate. So our work, which is the first theory of metal deposition from an atomic point of view, is able to provide important insights into the details of the mechanism.

Technical Section

DFT Calculations

All quantum chemical calculations were performed using the DACAPO code,[24] which utilizes an iterative scheme to self-consistently solve the Kohn–Sham equations of density functional theory. A plane-wave basis set was used to expand the electronic wavefunctions, and the inner electrons were represented by ultrasoft pseudopotentials,[25] which allow the use of a low-energy cut-off for the plane-wave basis set. An energy cut-off of 400 eV, dictated by the pseudopotential of the metal, was used in all calculations. The electron–electron exchange and correlation interactions were treated with the generalized gradient approximation (GGA) as described by Perdew et al.[26] The Brillouin-zone integration was performed using an $8\times8\times1$ k-point Monkhorst–Pack grid[27] that corresponds to the (1×1) surface unit cell. The surfaces were modeled by using a (2×2) supercell with four metal layers and eight layers of vacuum. For Cu, we obtained a lattice constant of 3.66 Å that is in good agreement with the experimental value of 3.61 Å; for Zn we obtained lattice constant of 2.64 Å and $c/a=1.92$—the experimental values are 2.66 Å and $c/a=1.86$. Dipole correction was used to avoid slab–slab interactions.[28] The first two layers were allowed to relax, while the bottom two layers were fixed at the calculated nearest-neighbor distance. The optimized surfaces (prerelaxed) in the absence of the corresponding atom (Zn or Cu) were used as input data to carry out the calculations to study the metal deposition. For each system, we performed a series of calculations for a single atom adsorbed on the hollow site, and varied its separation from the surface. The prerelaxed surface was kept fixed while the Zn or Cu atom was allowed to relax within the *xy* coordinates during these calculations. At each position we calculated the adsorption energy, and the DOS projected onto the 4s orbital of zinc or copper. The energy to detach an atom from the kink site position and to move it to the terrace was obtained from the nudged elastic-band method.[29] To perform this calculation the surface was modeled by a (4×4) supercell with four layers. The top layer was used to create the defect. All other parameters were the same as for the DFT calculations.

Molecular Dynamics

Purely classical molecular dynamics were performed using the large-scale atomic/molecular massively parallel simulator (LAMMPS)

code.[30] The system consisted of a Cu(100) slab modeled by three metal layers (4.66 Å thickness), an ensemble of 470 water molecules, and the Cu ion initially located in the bulk of the water. Periodic boundary conditions were used only in the *xy* directions. The dimensions of the box were $26.38\times26.38\times24.92$ Å^3. The correction for the electrostatic long-range interactions was done by using a pppm/cg solver. The temperature was set to 298 K using the NVT canonical ensemble. The data for Zn deposition were taken from ref. [8].

To calculate the energy of hydration for Zn^+ a cubic box of 24.70 Å of length was used and the ion was solvated by 470 water molecules. An isothermal–isobaric (NPT) ensemble was used in the simulation with the temperature set to 298 K. During this simulation the charge of the ion was gradually adjusted to compute the free-energy difference.

The following interactions were used: The parameters for the interaction between the water molecules with the copper surface were taken from a previous work;[31] the interactions between the water molecules in the bulk and between the copper ion with the water were specified by well-established Lennard–Jones potentials. For the water, we used the extended simple point charge (SPC/E) model and the corresponding parameters for the oxygen and hydrogen were taken from Yoshida et al.[32] The parameters for Cu ion–O interaction were taken from Fulton et al.[33] The corresponding interaction parameters for Zn ion–O were taken from Li et al.[34]

The weighted histogram analysis method (WHAM) code developed by Grossfield[35] was used to obtain the potential of mean force from a series of umbrella sampling simulations. A total of 40 umbrella samplings were performed. First we carried out an equilibration run of 500 ps, and then each sample ran for 200 ps, with a time-step of 2.0 fs.

Theoretical Framework

We present our model for the case where the two electrons that are transferred share the same orbital, as in the deposition of Zn. The case of Cu is simpler: the first electron transfer involves a d orbital and takes place in the outer-sphere mode, the second one involves one electron in the 4s orbital. In the range of distances of interest spin polarization was not observed and the model is equivalent to that employed for hydrogen evolution.[13]

The formalism is the same as that presented previously,[36,37] and consists of a combination of electron-transfer theory with spin polarization[2] and DFT. The only new feature is the use of the pmfs obtained from molecular dynamics to obtain the interactions with the solvent.

It is convenient to split the model Hamiltonian into several parts. We start with the spin orbitals for the electrons on the reactant [Eq. (9)]:

$$H_e = \sum_\sigma \left(\varepsilon_a n_{a,\sigma} + U n_{a,\sigma} n_{a,-\sigma}\right) \tag{9}$$

where ε_a is the energy of the valence orbital, n_a the corresponding number operator, U the Coulomb repulsion between two electrons on the same orbital, and σ denotes the spin index. The metal and its interaction with the reactant is represented by Equation (10):

$$H_{met} = \sum_{k,\sigma}\left[\varepsilon_k n_{k,\sigma} + \left(V_{a,k} c^+_{k,\sigma} c_{a,\sigma} + \text{h.c.}\right)\right] \tag{10}$$

The quasimomentum *k* labels the states on the metal, the matrix elements $V_{a,k}$ couple the metal states with the reactant, c^+ and *c* denote creation and annihilation operators, and h.c. is the Hermitian conjugate. The sum of the Hamiltonians Eqs. (9) and (10) is the Anderson–Newns model.[38,39]

The solvent is modeled as a phonon bath which interacts linearly with the charge on the reactant [Eq. (11)]:

$$H_{ph} = \frac{1}{2}\sum_\nu \hbar\omega_\nu\left(p_\nu^2 + q_\nu^2\right) + \left[z - \sum_\sigma n_{a,\sigma}\right]\left[\sum_\nu \hbar\omega_\nu g_\nu q_\nu\right] \tag{11}$$

Here, p_ν and q_ν denote the dimensionless momenta and coordinates of the phonons of frequencies ω_ν, *z* is the charge number, and g_ν denotes the coupling constants.

As in all theories of electron transfer, the phonon bath represents the slow solvent modes. As long as these modes are in the classical range, they can be represented by one effective solvent coordinate *q*, which we normalize in the following way: When the solvent coordinate takes on the value *q*, it is in equilibrium with a charge of $-q$ on the reactant. The reduction to one effective mode and the normalization are discussed by Schmickler and Santos in ref. [20]. After transforming to a single coordinate, the solvent part of the Hamiltonian reads [Eq. (12)]:

$$H_{sol} = \lambda(q^2 + p^2) + (z - n_{a,\sigma} - n_{a,\sigma})2\lambda q \tag{12}$$

where $\lambda = \sum_\nu \hbar\omega_\nu g_\nu^2/2$ is the energy of reorganization of the solvent. The effect of the fast solvent modes is discussed below.

The sum of the terms in Equations (9) to (11) is the electronic part of the Hamiltonian. We divided the electronic states on the metal into two bands, the d and the sp band, and assumed that the coupling constants are constant throughout the band and can be replaced by two coupling values, V_d and V_{sp}. This division allowed us to define two chemisorption functions for each band [Eq. (13)]:

$$\begin{aligned}\Delta_x(\varepsilon) &= \pi|V_x|^2\sum_k \delta(\varepsilon - \varepsilon_k)\\ \Lambda_x(\varepsilon) &= |V_x|^2\,\mathrm{P}\left(\sum_k \frac{1}{\varepsilon - \varepsilon_k}\right)\end{aligned} \tag{13}$$

where P denotes the principle part and the index *x* stands either for the d or the sp band.

In order to separate the two spin states on the reactant, we employed the Hartree–Fock approximation [Eq. (14)]:

$$U n_{a,\sigma} n_{a,-\sigma} \approx U n_{a,\sigma}\langle n_{a,-\sigma}\rangle + U\langle n_{a,-\sigma}\rangle n_{a,-\sigma} - U\langle n_{a,\sigma}\rangle\langle n_{a,-\sigma}\rangle \tag{14}$$

This approximation allowed us to calculate the Green's functions and the corresponding densities of states (DOS) for the two spin states [Eq. (15)]:

$$\rho_{a,\sigma}(\varepsilon) = \frac{1}{\pi}\frac{\Delta(\varepsilon)}{\left[\varepsilon - (\varepsilon_a + \Lambda(\varepsilon) + U\langle n_{a,-\sigma}\rangle - 2\lambda q)\right]^2 + \Delta(\varepsilon)^2} \tag{15}$$

where Δ and Λ contain contributions from the d and sp bands. The occupation probabilities $\langle n_{a,\sigma}\rangle$ are obtained by integrating the DOS up to the Fermi level, which we took as our energy zero [Eq. (16)]:

$$\langle n_{a,\sigma}\rangle = \int_{-\infty}^{0} \rho_{a,\sigma}(\varepsilon)\, d\varepsilon \tag{16}$$

As the DOS of one spin contains the occupation probability of the other, Equations (15) and (16) are a set of two equations which have to be solved self-consistently. Note that the DOS, and hence the occupation probabilities, depend explicitly on the solvent coordinate q. The electronic part of the energy is then given by [Eq. (17)]:

$$E_{el}(q) = \left[\sum_{\sigma}\int_{-\infty}^{0} \rho_{a,\sigma}(\varepsilon)\, \varepsilon\, d\varepsilon\right] - U\langle n_{a,\sigma}\rangle\langle n_{a,-\sigma}\rangle \tag{17}$$

In order to calculate free-energy surfaces, we need the coupling constants, V_d, V_{sp}, and the electronic energy, ε_a, as a function of the distance. For this purpose, we have calculated the DOS of sp and the d band of the metal, and both the energy and the DOS of the metal atom at various distances by DFT. These calculations were performed with spin polarization, but over the distances required, as shown in Figures 4 and 5, spin polarization did not occur. The three parameters were obtained by fitting the DOS obtained from DFT to the form of Equation (15), setting $q=0$. The details are explained in [13].

The Coulomb repulsion U was obtained by performing DFT calculations both for the atom and the ion as a function of the distance. Ionization was achieved by applying a suitable electric field. Details of this procedure are given in the appendix of [36].

In addition, we needed the reorganization energy as a function of the distance. This result was obtained in the following way: The energy of solvation of the monovalent ion, as a function of the distance, is given by the bulk value plus the potential of mean force. As the Pekar[14] factor for water is about 1/2, half of the solvation energy gives λ and the other half is the interaction λ_f with the fast solvent modes. The latter modes also contribute to the total energy. Because these modes are fast, their contribution to the energy is proportional to the square of the charge [Eq. (18)]:

$$E_f = (z - \langle n_{a,\sigma}\rangle - \langle n_{a,\sigma}\rangle)^2 \lambda_f \tag{18}$$

As can be seen from Equation (12) the slow solvent modes also contribute a term that is not included in the DOS of Equation (15) and hence not in the electronic energy [Eq. (19)]:

$$E_s = \lambda q^2 + 2z\lambda q \tag{19}$$

The sum $E_{el}+E_f+E_s$ is the energy obtained from Anderson–Newns theory. The correction for many-body effects is the same as described in ref. [13]: We calculated the electronic energy $E_{el}(q=0)$ without the solvent and compared it with the electronic energy obtained by DFT [Eq. (20)]:

$$\Delta E(q=0) = E_{DFT} - E_{el}(q=0) \tag{20}$$

For $q \neq 0$ we assumed that this error is proportional to the occupancy of the valence orbital [Eq. (21)]:

$$\Delta E(q) = \Delta E(q=0) \times (\langle n_{a,\sigma}\rangle + \langle n_{a,-\sigma}\rangle)/2 \tag{21}$$

This term was added to the electronic energy calculated from the extended Anderson–Newns formalism. Equation (21) is a natural interpolation between the limiting cases of an empty and a completely filled orbital, for which it is correct by construction.

We believe that the explicit calculation of the solvation effects from molecular dynamics constitutes a significant improvement of our model and leads to more reliable results.

Keywords: corrosion · density functional theory · electron transfer · metal deposition · molecular dynamics

[1] W. Schmickler, *Chem. Phys. Lett.* **1995**, *237*, 152.
[2] W. Schmickler, *Electrochim. Acta* **1996**, *41*, 2329.
[3] M. T. M. Koper, W. Schmickler, *J. Electroanal. Chem.* **1998**, *450*, 83.
[4] O. Pecina, W. Schmickler, *J. Electroanal. Chem.* **1998**, *450*, 303.
[5] R. R. Nazmutdinov, W. Schmickler, A. M. Kuznetsov, *Chem. Phys.* **2005**, *310*, 257.
[6] L. M. C. Pinto, E. Spohr, P. Quaino, E. Santos, W. Schmickler, *Angew. Chem.* **2013**, *125*, 8037; *Angew. Chem. Int. Ed.* **2013**, *52*, 7883.
[7] H. Gerischer, *Z. Elektrochem.* **1958**, *62*, 256.
[8] O. Pecina, W. Schmickler, *Chem. Phys.* **2000**, *252*, 349.
[9] R. A. Marcus, *J. Chem. Phys.* **1956**, *24*, 966.
[10] *Standard Potentials in Aqueous Solutions* (Eds.: A. Bard, R. Parsons, J. Jordan), Marcel Dekker, New York, **1985**.
[11] O. Pecina, W. Schmickler, E. Spohr, *J. Electroanal. Chem.* **1995**, *394*, 29.
[12] C. Hartnig, M. T. M. Koper, *J. Am. Chem. Soc.* **2003**, *125*, 9840.
[13] E. Santos, A. Lundin, K. Pötting, P. Quaino, W. Schmickler, *Phys. Rev. B* **2009**, *79*, 235436.
[14] S. I. Pekar, *Untersuchungen über die Elektronentheorie der Kristalle*, Akademie-Verlag, Berlin, **1954**, p. 184.
[15] C. Hartnig, M. T. M. Koper, *J. Electroanal. Chem.* **2002**, *532*, 165.
[16] N. S. Hush, *J. Chem. Phys.* **1958**, *28*, 962.
[17] W. Schmickler, E. Santos, *Interfacial Electrochemistry*, Springer, New York, **2010**, pp. 270.
[18] R. Burrows, K. L. Dick, I. A. Harrison, *Electrochim. Acta* **1976**, *21*, 81.
[19] R. Burrows, J. A. Harrison, J. Thompson, *J. Electroanal. Chem.* **1975**, *58*, 241.
[20] W. Schmickler, E. Santos, *Interfacial Electrochemistry*, Springer, New York, **2010**, pp. 31.
[21] E. Gileadi, *J. Electroanal. Chem.* **2011**, *660*, 247.
[22] E. Gileadi, *J. Electroanal. Chem.* **2002**, *532*, 181.
[23] M. Sluyters-Rehbach, J. S. M. C. Breukel, J. H. Sluyters, *J. Electroanal. Chem.* **1968**, *19*, 85, and references therein.
[24] B. Hammer, L. B. Hansen, J. K. Nørskov, *Phys. Rev. B* **1999**, *59*, 7413.
[25] D. Vanderbilt, *Phys. Rev. B* **1990**, *41*, 7892.
[26] J. P. Perdew, K. Burke, M. Ernzerhof, *Phys. Rev. Lett.* **1996**, *77*, 3865.
[27] H. J. Monkhorst, J. D. Pack, *Phys. Rev. B* **1976**, *13*, 5188.
[28] L. Bengtsson, *Phys. Rev. B* **1999**, *59*, 12301.
[29] G. Henkelman, B. P. Uberuaga, H. Jónsson, *J. Chem. Phys.* **2000**, *113*, 9901; G. Henkelman, H. Jónsson, *J. Chem. Phys.* **2000**, *113*, 9978.
[30] S. Plimpton, *J. Comput. Phys.* **1995**, *117*, 1.
[31] S. Frank, C. Hartnig, A. Groß, W. Schmickler, *ChemPhysChem* **2008**, *9*, 1371.
[32] K. Yoshida, T. Yamaguchi, A. Kovalenko, F. Hirata, *J. Phys. Chem. B* **2002**, *106*, 5042.
[33] J. L. Fulton, M. M. Hoffmann, J. G. Darab, B. J. Palmer, E. A. Stern, *J. Phys. Chem. A* **2000**, *104*, 11651.
[34] X. Li, Y. Tu, H. Tian, H. Ågren, *J. Chem. Phys.* **2010**, *132*, 104505.
[35] A. Grossfield, "WHAM: an implementation of the weighted histogram analysis method", version 2.0.6, can be found under http://membrane.urmc.rochester.edu/content/wham.
[36] E. Santos, P. Quaino, W. Schmickler, *Phys. Chem. Chem. Phys.* **2012**, *14*, 11224, and references therein.
[37] P. Quaino, N. B. Luque, R. Nazmutdinov, E. Santos, W. Schmickler, *Angew. Chem.* **2012**, *124*, 13171; *Angew. Chem. Int. Ed.* **2012**, *51*, 12997.
[38] P. W. Anderson, *Phys. Rev.* **1961**, *124*, 41.
[39] D. M. Newns, *Phys. Rev.* **1969**, *178*, 1123.

Received: September 15, 2013
Published online on December 2, 2013